ELINVO (Electronics, Informatics, and Vocational Education), November 2021;6(2): 149-156
ISSN 2580-6424 (printed), ISSN 2477-2399 (online,) DOI: https://doi.org/10.21831/elinvo.v6i2.43409

Switching Algorithm for SVPWM Inverter in Induction Motor Drive System on Electric Vehicle Applications

Bayu Praharsena[1], Mohammad Jauhari[2], Era Purwanto[3], Mentari Putri Jati[4], Angga Wahyu Aditya[5], Aries Alfian Prasetyo[6]
[1,2,6]Politeknik Negeri Madura, [3]Politeknik Elektronika Negeri Surabaya,
[4]Universitas Negeri Yogyakarta, [5]Politeknik Negeri Balikpapan
bayu@poltera.ac.id

ABSTRACT

Electric cars are the way to reduce global warming and fuel shortages. Performance variable speed drive is needed for various drive electric vehicle applications. Unfortunately, high performance is still being investigated with a variety of drive systems. This paper presents a design, analysis, and implementation of the SV-PWM inverter motor drive system. The SV-PWM algorithm in design using Matlab, to analyze the system include signal response, THD-V, THD-I. All algorithms are embedded in STM32F4, as the main controller. The hardware uses a 3-phase motor control Steval power module.

Keywords*:* Induction Motor, SV-PWM inverter, THD-V, THD-I, STM32F4

INTRODUCTION

About 84% of global energy is generated by fossil fuels[1] which generates gases when it is burned. The possible solution to reduce environmental pollution, promote fossil fuels and all energy consumption in electrical form. EVs technology becomes the solution to replacing ICE-based vehicles. EV will have the potential to solve the problems associated with energy resources, environmental pollution, and reduce oil usage. More than 1 million electric cars have been produced, based on Global EV outlook 2016 shows that by 2015 China has become a major market worldwide. China is the largest developer globally in EV, e-scooters, and e-busses [2].

Three-phase squirrel-cage induction motors (IMs) are suitable for use in EV for reliability, low maintenance, low cost, and robustness [3][4][5][6]. In the industrial sector, IMs are applied for many fixed-speed, but in the transportation sector, EVs should be operated at variable speeds. In this condition, EVs must be used for variable-frequency drives (VFDs).

Compared to the SPWM method, SVPWM is more suitable for VFDs EV, with lower harmonics and higher output voltages [7][8]. EV requires instant and significant speed changes, so it is necessary to observe the SVPWM signal response. The proposed design is tested by experiment, using Yokogawa scope coder which is integrated with Matlab to observe any induction motor speed change response.

The main objective of this paper is to analyze SVPWM inverters in various aspects such as harmonic, speed response, inverter output signal.

PRINCIPLE OF SPACE VECTOR MODULATION

Three voltage variablesV_a,V_b and V_c are calculated by using inverse-Clarke transformation to obtain$V_{\alpha(t)}$ and$V_{\beta(t)}$. Where $V_{\alpha(t)}$ dan $V_{\beta(t)}$ form an angle of 90°. The SVPWM algorithm is calculated on the STM32F4 microcontroller, generated the switching on each phase is generated based on the standard vector voltage in Figure 1. It

assumes that $V_{a(t)}$,$V_{b(t)}$ and $V_{c(t)}$ is a logical vector that is located in the vector sector.

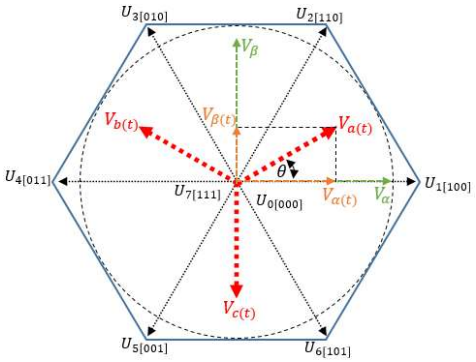

Figure 1. Standard vector for SV-PWM

The area between the standard vector U_1 and U_2 (Figure 1). At the ideal state $V_s = V_a = V_b = V_c$ is the resultant vector of $V_{\alpha(t)}$ and $V_{\beta(t)}$, it's a two boundary vector on each phase. So the value of V_s to the time change as Equation 1.

$$V_{s(t)} = \sqrt{{V_{\alpha(t)}}^2 + {V_{\beta(t)}}^2} \quad (1)$$

Any changes $V_{\alpha(t)}$ and $V_{\beta(t)}$, the logical state of the period as Equation 2.

$$T_{\alpha(t)} = T_p \frac{|V_{\alpha(t)}|}{|V_{a(max)}|}; T_{\beta(t)} = T_p \frac{|V_{\beta(t)}|}{|V_{a(max)}|} \quad (2)$$

To represent the value of $T_{\alpha(t)}$ and $T_{\beta(t)}$, the pulse pattern must correspond to the vector diagram in Figure 1 then calculate the boundary magnitude $T_{\alpha(t)}$ and $T_{\beta(t)}$ can be performed by using the following Equation 3.

$$V_{\alpha(t)} = \frac{2}{\sqrt{3}}|V_{s(t)}| \sin(\theta) ;$$
$$V_{\beta(t)} = \frac{2}{\sqrt{3}}|V_{s(t)}| \sin(60° - \theta) \quad (3)$$

If one full period is taken during the time T_p on each vector with a maximum modulation of $\frac{2}{3}U_{dc}$ from the standard vector, is described as Equation 4.

$$|V_s| = |U_1| = \ldots = |U_7| = \frac{2}{3}V_{dc} \quad (4)$$

The switching time and the configuration of the switch state for each IGBT are calculated in the microcontroller. C code consist of the magnitude of reference, the angle of the reference (θ), and the timer signal for comparison. Here's how to implement $T_{\alpha(t)}$ and $T_{\beta(t)}$, the microcontroller is programmed as Equation 5.

$$T_{\alpha(t)} = \frac{\sqrt{3}}{V_{max}} V_{ref} \sin\left(\frac{\pi}{3} - \theta\right) T_s$$
$$T_{\beta(t)} = \frac{\sqrt{3}}{V_{max}} V_{ref} \sin(\theta)\, T_s \quad (5)$$

Where T_s is a sampling time microcontroller, which can be calculated as Equation 6.

$$T_s = \left(\frac{f_{coreclock}}{2 * f_{triangle}}\right) - 1$$
$$T_s = \left(\frac{f_{coreclock}}{2 * f_{modulation} * f_{\max\_operation}}\right) - 1 \quad (6)$$

Where $f_{coreclock}$ used on STM32F4 is $168\, e^6 Hz$. So if writing in each sector 1 is as Equation 7.

$$V_{a(t)} = \frac{T_s}{2} - T_{\alpha(t)} - T_{\beta(t)}$$
$$V_{b(t)} = \frac{T_s}{2} + T_{\alpha(t)} - T_{\beta(t)} \quad (7)$$
$$V_{c(t)} = \frac{T_s}{2} + T_{\alpha(t)} + T_{\beta(t)}$$

Figure 2 represents the output signal of the microcontroller forming the SVPWM signal used to control each IGBT. The peak-to-peak signal voltage is 2.87Volt.

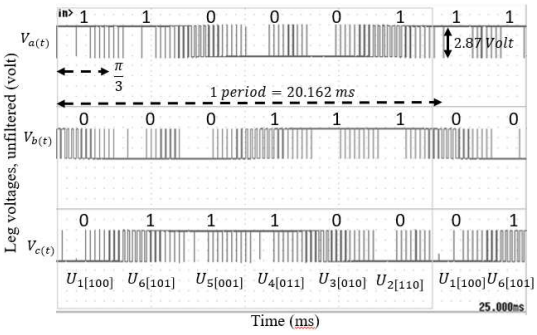

Figure 2. SV-PWM signal (unfiltered)

Numbering on each phase is shown as a vector change based on Figure 1. The duty cycle is set by an equation, with the angular shift of $\frac{\pi}{3}$, which is implemented with a lag of 6,717ms.The following figure is a 500Hz filtered SVPWM signal.

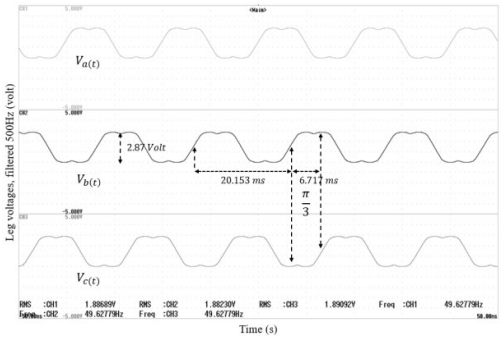

Figure 3. SV-PWM filtered.

This study uses a 3-phase VSI circuit that is implemented on IGBT intelligent power module STGIPS20C60. The module is a DC to AC inverter that generates a 3-phase waveform for driving 3-phase IMs. The reason for using the module, because this module is designed to be compatible with single-phase supply, from 90Vac to 285Vac, so it is suitable for used on the lab scale.

EXPERIMENT SETUP

The power supply for this system is designed as a wide range converter, the range input voltage is from 90VAC up to 285VAC.

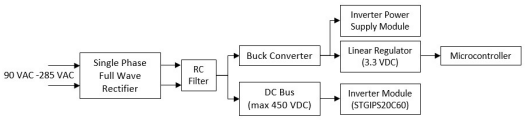

Figure 4. The block diagram of the experimental system

The system uses Three-Phase Three-Wire (3P3W) relationship, where 4 channels oscilloscope that receives two pairs of voltage and current signals can be wired.

A six state signal modulation is controlled by microcontroller, this signal is used to generate the firing pulse to control the operation of the inverter. If we translated in the form of 3 phase SVPWM inverter circuit as shown.

In the 3P VSI circuit consists of 2 sectors, the IGBT high side and the low side, the low side is complementary to the high side. This means that the SVPWM signal generated when the high side is worth 1 then on the low side is 0, but the condition must be given time lag. Pause between the high side and low side is encapsulated on the microcontroller. Each IGBT has an antiparallel diode, its function as a protection.

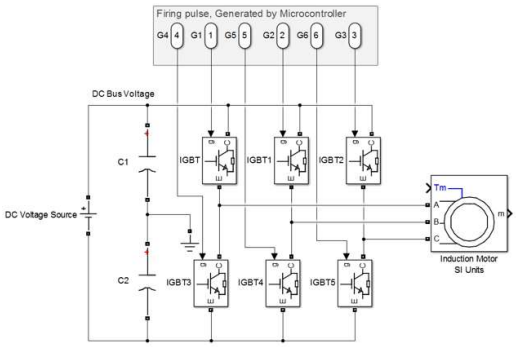

Figure 5. Power circuit topology of a 3-Phase VSI

If it is assumed that each phase is in a balanced condition, then the equation is as Equation 8.

$$V_{an} = V_{max}\cos(\omega t)$$
$$V_{bn} = V_{max}\cos\left(\omega t - \frac{2\pi}{3}\right)$$
$$V_{cn} = V_{max}\cos\left(\omega t + \frac{2\pi}{3}\right) \quad (8)$$
$$\bar{V} = \frac{2}{3}[V_{an} + aV_{bn} + a^2V_{cn}]$$

Where, V_{an}, V_{bn}, V_{cn} are the voltages in phases A, B, and C, whereas $\frac{2\pi}{3}$ represents the shift of each phase.

In this experiment, a speed sensor is needed to observe the IM response. We use a Photodiode and Led to detect the rotor position. The sensor output value will compare with comparator IC LM-393 to generate a pulse. Rotor shaft design with a black and white condition, if sensor detects white area comparator generates a high level pulse and vice versa. This measurement has been done using the frequency counter, it is based on counting the number pulses in a given time for one rotation. The system counts the number of pulses N_r appearing from the pulse generator over an interval T_r. This method can count the rotor frequency from the signal received if the number of pulse per revolution of the sensor is N. The rotation frequency in Hz is as Equation 9.

$$F = \frac{N_r}{N.T_r} \quad (9)$$

In high frequency, the comparator will generate pulse add with noise. noise will make error measurement for calculating rotor frequency. The system must commit a counting error of a pulse, then we get the measurement error for a single rotation is written in Equation 10.

$$Error(N_r)\% = \frac{100.F(N_r+1) - F(N_r)}{F(N_r)} \quad (10)$$

As the result, the frequency number of the shaft rotor can be counted from pulse counted. The rotor speed can be graphed on the resulting experiment.

EXPERIMENTAL RESULTS

All experimental data is transmitted to Matlab, to be monitored and processed for analysis. The following switching algorithm, its will show how a microcontroller produces the eight standard vectors from the arbitrary stator voltage vector[9]. If observed in the SVPWM inverter output signal, the voltage wave based on the standard vector is as follows. Figure 6 shows the experimental setup.

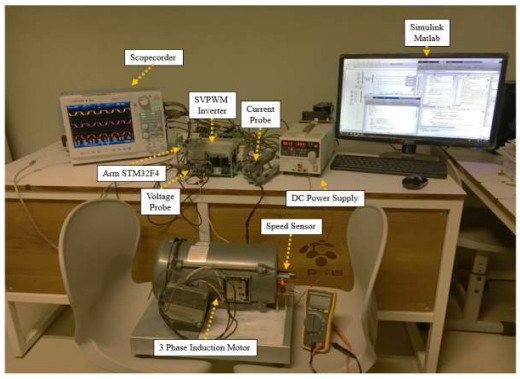

Figure. 6 Experiment Setup

Current values of all measured quantities and the value of the calculated power can be the plot in Matlab. Using Matlab we can analyze the performance of SV-PWM inverter for an induction motor implemented on EV. We can plot speed, phase current, RMS phase current, RMS phase voltage, and power. Finally, fig shows the appearance of the speed response, current, voltage as a function of power output

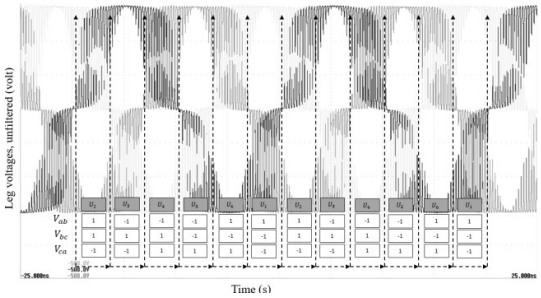

Figure7. The signal output voltage of the SV-PWM inverter

Harmonic components of the SVPWM signal are given, using FFT series expression. It appears that at the fundamental voltage (50Hz) 302.6V with THD-v equal to 35.29%.

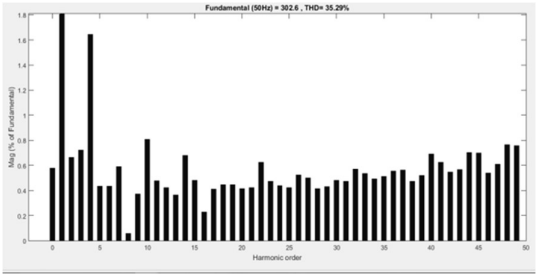

Figure8. THD-V of the SV-PWM inverter

Using Matlab, we computed harmonic voltage order. In this graph correspondence of the output voltage signal from SV-PWM inverter.

The following is a Harmonic order, showing the fundamental current (50Hz) of 0.171A and THD-I is 102.77%. Using scopecorder can observe dead-time. It is a time lag that automatically generated microcontroller when there is a change of positive and negative side. Based on experiments, dead-time on SVPWM inverter 200us, of total time in one full wave of 20ms. Dead-time is necessary to prevent short-circuit on high-side IGBT and low-side IGBT. When 3P IMs connect the stator of an IMs to a 3P SV-PWM inverter, with the load. The stator creating the revolving field cuts across the rotor bar and induces a voltage in all of them, by a number of N poles.

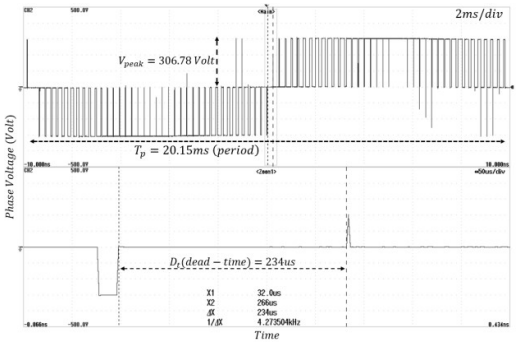

Figure9. Deadtime representation of the SV-PWM inverter

Because the rotor bars are short-circuited, the current carrying conductors of the stator have created a flux[10], consequently, they all experience a strong mechanical force[11]. The forces tend to drag the rotor along with the revolving field. Based on the experiment, the starting current is very high. It happens when the magnetic field is created by the stator, they are therefore producing a strong mechanical force to drive the rotor bar from 0 rpm to reference rpm.

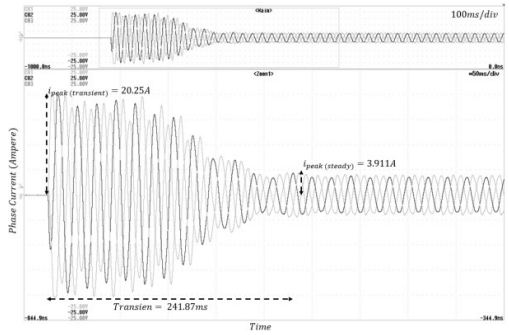

Figure 9. The signal output current of the SV-PWM inverter

Electric cars should be able to operate with a high response, so when the motor start becomes an interesting topic to be observed. The following is the current waveform, voltage, and rpm of the induction motor observed using the oscilloscope.

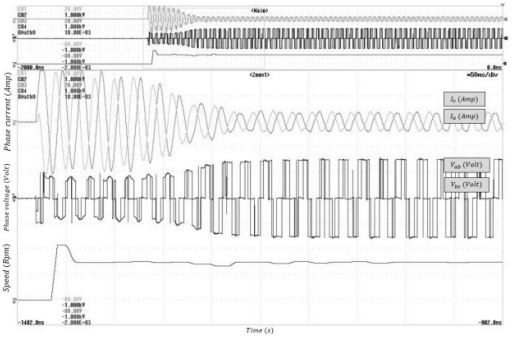

Figure 11. current response, voltage response, speed response.

The initial response of the motor in the starting condition is 6,606 ms, from 0 rpm it reaches 2163 Rpm. The motor takes 42.894ms to reach steady state, from 0 rpm to 1483rpm. The motor starts up to 48.05% of the reference speed. Overshoot very influential on the user when driving electric cars, overshoot may result buffeting when the car starting.

Every data in the system is monitored using Matlab to observe the system response and its effect on EVs. The picture below shows the speed response that is read from the speed sensor. The signal from the sensor is filtered by Matlab and displayed again in the form of a graph.

when the stator is supplied from the SV-PWM inverter, it appears that the motor does not respond immediately but there is a delay of 15,903ms. This is the process of supplying the stator to induce the rotor to generate flux. Then there is an increase in current which is high enough so that the motor can rotate from rest to moving. To induce the rotor so that the shaft can move requires a fairly high starting current of 9,157A. while in steady state conditions only requires a current of 2.285A per phase. Based on these tests, IMs require starting current to reach 300.74% of steady state current. This condition greatly affects the power consumption of the battery, the lifetime of the motor, and the inverter.

The motor is tested with a significant change in speed. When observed, the current signal oscillates until it reaches a steady state condition within 189.89ms. Much slower than

the motor rotational speed response. The mechanical load is one of the aspects why IMs stabilize quickly, while the motor starting current is influenced by the controller and inverter devices. The current response of the inverter within 189.89ms has no impact on the user when operating an electric car. On the other hand, the inverter must be able to respond with various speed variations instructed by the driver.

We tried to measure the power required for starting an induction motor. Based on the graph in Figure shows that when the inverter starts to supply the motor, the motor does not immediately rotate but is stationary. In this case, the rotor seems to be short-circuited so that it requires a high current to start it. When the current increases, a voltage drop occurs, but the inverter output power increases to produce a sufficiently high initial motor power. It appears that the response of the motor power increases until the motor has an increase in rpm. When the motor starts to move, the motor power will decrease in proportion to the decreasing current. In steady state conditions, the motor power is very small, because there is a moment of inertia stored by the mechanical load on the electric car.

In the starting-sector classification, it is shown in 5 conditions. Sector A is the initial power response used to generate the initial induction when the IMs rotor shaft is still at rest. the phase angle reveals that the rotor current is also an inductive and lagging current, rotor lagging for 14.99ms. Sector B is the response of the motor shaft starting to move. In this condition, the stator current will increase until the rotor speed reaches the rated speed. This response greatly affects the inverter to variations in speed changes when the user drives the EVs. The input stator current will vary with the motor slip or rotor speed, at this condition lasts 38.7ms. The larger starting current occurs when s= 1 (100% slip). Therefore, the mechanical losses are assumed zero.

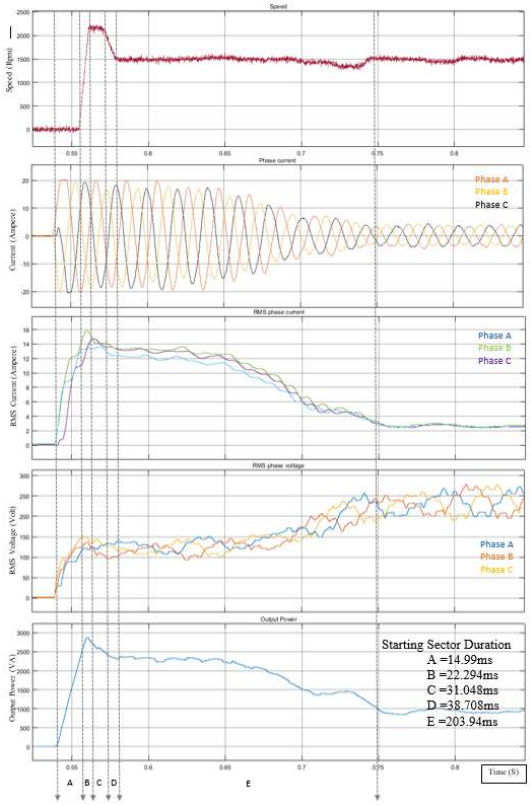

Figure 12. response

The SV-PWM inverter produces a higher consumption of DC-link voltage but has a lower THD-I than the SPWM inverter[12].

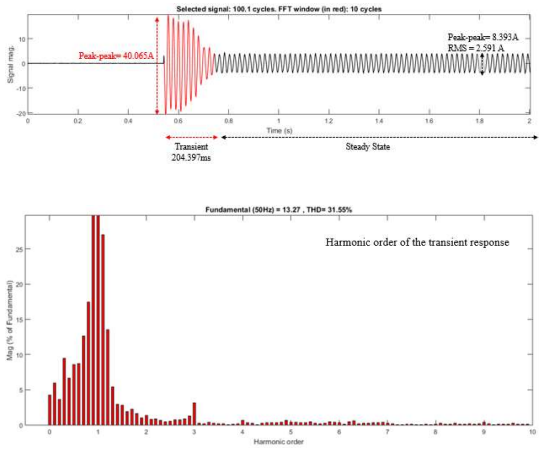

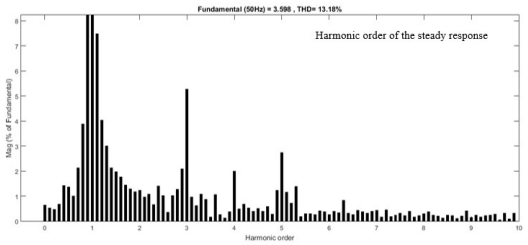

Figure 13. THD-I and THD-V response

The starting current should be kept low to avoid overheating of the motor and excessive voltage drops in the inverter. Hence the starting currents should be reduced, there are many ways used on an induction motor.

SV-PWM inverter generates supply for IMs, these voltages frequently are unbalanced or even harmonic-rich. If the current carry on IMs by SV-PWM inverter contain harmonics, these will interfere with the resulting current, so the current harmonic has a ratio summing value. To determine the effect of non-sinusoidal currents is expressed in Equation 11.

$$i_{a(t)} = \sum_{n=1}^{\infty} i_{an} \exp(nj\omega_s t)\exp(-nj\theta_n)$$
$$i_{b(t)} = \sum_{n=1}^{\infty} i_{bn} \exp(nj\omega_s t) \exp(-nj\theta_n) \exp\left(-nj\frac{2\pi}{3}\right) \quad (11)$$
$$i_{c(t)} = \sum_{n=1}^{\infty} i_{cn} \exp(nj\omega_s t) \exp(-nj\theta_n) \left(nj\frac{2\pi}{3}\right)$$

Where θ_n is the phase difference between the voltage and the current signal.

To study the IMs behaviors, the starting characteristic and transient response should be considered. The motor is tested with several variations of rpm, the following is the current of the motor while operating at some speed. Pada kondisi low speed mode, motor mengkonsumsi daya yang lebih tinggi bila dibandingkan pada rate speed. The amount of power consumed by the asynchronous machine depends on its load torque.

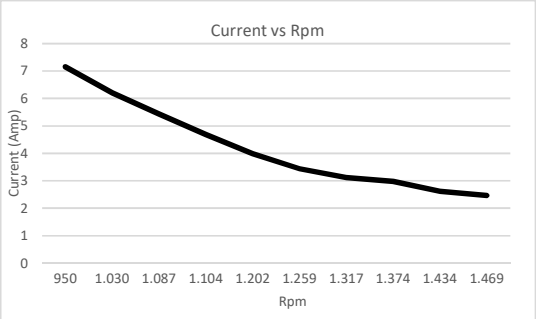

Fig 14. Speed vs Current motor.

CONCLUSIONS

This study has sufficient insight into the complexity of SVPWM on standard vector regions. Using microcontroller and VSI Steval power module successfully run the induction motor well. Motor performance can be observed on a graph of current response, voltage, and motor rpm. The motor response characteristic is important for practical purposes because it can be used to estimate motor performance. When the motor start condition can respond in a short time. So suitable for use for speed variations on electric cars.

BIBLIOGRAPHY

[1] H. Abu-Rub, M. Malinowski e K. Al-Haddad, Power Electronics for renewable energy systems, transportation and industrial applications, United Kingdom: IEEE Press and John Wiley & Sons Ltd, 2014.

[2] "Global EV Outlook 2016, beyond one million electric cars," IEA, Paris, 2016.

[3] A. khajepour, S. Fallah e A. Goodarzi, Electric and Hybrid Vehicles, Technologies, Modeling and Control: a Mechatronic Approach, United Kingdom: John Wiley & Sons Ltd, 2014.

[4] M. A. Jirdehi e A. Rezaei, "Parameters estimation of squirrel-cage induction motors using ANN and ANFIS," *Alexandria Engineer Journal,* pp. 357-368, 2016.

[5] N. Jirasuwankul, "Simulation of energy

efficiency improvement in induction motor drive by fuzzy logic based temperature compensation," em *3rd International Conference on Energy and Environment Research, ICEER 2016*, Barcelona, Spain, 2017.

[6] L. W. Silva, A. M. Nogueira Lima e A. Oliveira, "A method for measuring torque of squirrel-cage induction motors without any mechanical sensor," *IEEE transaction on instrumentation and measurement,* pp. 1-9, 2014.

[7] R. A. a. K. Baskaran, "Implementation of Fuzzy PI Controller for Speed Control of Induction Motors Using FPGA," *Journal of Power Electronics,* pp. 65-71, 2009.

[8] k. k. kumar e v. kumar, "eksperimental investigation on space vector pulse width modulation based induction motor drive," em *Annual IEEE India Conference (INDICON)*, India, 2015.

[9] I. Ferdiansyah, M. Rizani Rusli, B. Praharsena, H. Toar, R. e E. Purwanto, "Speed Control of Three Phase Induction Motor Using Indirect Field Oriented Control Based on Real-Time Control System," em *2018 10th International Conference on Information Technology and Electrical Engineering (ICITEE)*, Bali, Indonesia, 2018.

[10] B. Praharsena, E. Purwanto, A. Jaya, M. Rizani Rusli, H. Toar, R. A. Aditya, I. Ferdiansyah e N. Eka Sandhi, "Evaluation of Hysteresis Loss Curve on 3 Phase Induction Motor by Using Cascade Feed Forward Neural Network," em *International Electronics Symposium on Engineering Technology and Applications (IES-ETA)*, Bali, Indonesia, 2018.

[11] B. Praharsena, E. Purwanto, A. Jaya, M. Rizani Rusli, H. Toar e R. , "Stator Flux Estimator Using Feed-Forward Neural Network for Evaluating Hysteresis Loss Curve in Three Phase Induction Motor," *EMITTER International Journal of Engineering Technology,* vol. 6, nº 1, 2018.

[12] A. A. Mansour, "novel SVPWM based on first order equation," *Journal of Electrical systems and information technology 2,* pp. 1976-206, 2015.